Deep-Sea Research II 118 (2015) 32–43

Contents lists available at ScienceDirect

Deep-Sea Research II

journal homepage: www.elsevier.com/locate/dsr2

Assessment of ocean color data records from MODIS-Aqua in the western Arctic Ocean

Joaquín E. Chaves [a,b,*], P. Jeremy Werdell [a], Christopher W. Proctor [a,b], Aimee R. Neeley [a,b], Scott A. Freeman [a,b], Crystal S. Thomas [a,b], Stanford B. Hooker [a]

[a] NASA Goddard Space Flight Space Center, Code 616, Greenbelt, MD 20771, USA
[b] Science Systems and Applications, Inc., Lanham, MD 20706, USA

ARTICLE INFO

Available online 11 March 2015

Keywords:
Ocean color
Satellite remote sensing
Arctic Ocean
Spatial distribution
Semi-analytical algorithms
Chlorophyll a
POC
CDOM
MODIS1

ABSTRACT

A broad suite of bio-optical and biogeochemical observations collected during the NASA-funded ICESCAPE expeditions to the western Arctic Ocean in 2010 and 2011 was used to validate ocean color satellite data products in this region, which is undergoing fast ecological changes in the context of a changing climate. Satellite-to-in situ match-ups for the MODIS instrument onboard Aqua (MODISA) were evaluated using standard NASA empirical and semi-analytical algorithms to estimate chlorophyll-*a* (C_a), spectral marine inherent optical properties, and particulate organic carbon (POC). Results for the empirical algorithms were compared with those from the semi-analytical Generalized Inherent Optical Property (GIOP) algorithm. The findings presented here showed that MODISA C_a estimates were positively biased relative to in situ measurements, in agreement with previous studies that have evaluated ocean color retrievals in the Arctic Ocean. These biases were reproduced using both satellite and in situ measured remote sensing reflectances, $R_{rs}(\lambda)$, indicating that estimation errors are derived from the application of the empirical algorithm and not by the observed radiometry. This disparity appears to be caused by contributions of high spectral absorption from chromophoric dissolved organic matter (CDOM), which is a well-documented feature of Arctic Ocean waters. The current MODISA empirical algorithm (OC3M) appears to attribute CDOM absorption in the blue region of the spectrum to phytoplankton absorption. In contrast, GIOP showed significant improvement over OC3M C_a estimates by effectively discriminating between phytoplankton and CDOM absorption. Additionally, executing GIOP with an expanded set of spectral bands derived from in situ radiometry, instead of just six MODISA bands, further improved the performance of absorption estimates. These findings reinforce previous suggestions that semi-analytical approaches will provide more reliable data records for Arctic studies than existing empirical methods. POC estimates showed no clear bias relative to in situ measurements, suggesting that the empirical algorithm better represents high latitude oceans with regards to the bio-optical signature of suspended particulate stocks.

1. Introduction

The Impacts of Climate change on the Eco-Systems and Chemistry of the Arctic Pacific Environment (ICESCAPE) Project took place during the boreal summer in 2010 and 2011, under the auspices of the National Aeronautics and Space Administration (NASA; https://www.espo.nasa.gov/icescape/). The multidisciplinary project's main objective was to improve our understanding of the impact of natural and anthropogenic climate change on the biogeochemistry and ecology of the Chukchi and Beaufort seas. Recently documented changes in summer ice cover (Comiso et al., 2008), accompanied by a transition from thick multiyear ice to a seascape increasingly dominated by thinner, first-year ice (Comiso, 2011; Kwok et al., 2009) have brought discernible modifications to the phenology of the Arctic Ocean region, such as earlier occurrences of the annual phytoplankton blooms (Kahru et al., 2011) and an overall increase in ocean net primary production (NPP) (Arrigo and van Dijken, 2011; Bélanger et al., 2013; Pabi et al., 2008; Petrenko et al., 2013). Climate models predict that ice cover changes may accelerate in the future, with the possible scenario of an ice-free Arctic during the summer months before the end of the century (Holland et al., 2006; Wang and Overland, 2009). The ICESCAPE program integrated a multi-disciplinary approach to enhance existing field data sets aimed at

* Corresponding author at: NASA Goddard Space Flight Space Center, Code 616, Greenbelt, MD 20771, USA.
E-mail address: joaquin.chaves@nasa.gov (J.E. Chaves).

http://dx.doi.org/10.1016/j.dsr2.2015.02.011
0967-0645/

supporting synthesis efforts to better understand the impacts of climate change on the ecology and biogeochemistry of the Chukchi and Beaufort Seas (e.g., Arrigo et al., 2012).

Ocean color satellite instruments provide valuable tools for advancing our understanding of the effects that these predicted changes would have on the Arctic Ocean. The remoteness of the western Arctic and the scarcity of in situ research platforms suitable for working year round in this seasonally ice-covered environment highlight the need for achieving climate-quality data records of ecologically relevant parameters from autonomous, remote-sensing platforms such as satellite instruments. The NASA Sea-viewing Wide Field-of-view Sensor (SeaWiFS) and Moderate Resolution Imaging Spectroradiometer onboard Aqua (MODISA), for example, provide estimates of the near surface concentration of chlorophyll-*a* (C_a, mg m^{-3}) and other marine ecological parameters such as marine inherent optical properties (IOPs; the spectral absorption and scattering properties of water column constituents and seawater itself). Time-series of C_a and IOPs can be valuable tools for assessing the changes in the ecology of Arctic Ocean in the context of a changing climate. Both can be used, for example, to infer the timing and succession of phytoplankton blooms and to generate estimates of NPP (Behrenfeld et al., 2005; Henson et al., 2010). Satellite instruments such as SeaWiFS and MODISA, therefore, provide biogeochemical data records of potential interest for Arctic studies on temporal and spatial scales that cannot be achieved by conventional aircraft and in situ sampling strategies in that region. Furthermore, SeaWiFS and MODISA operate in sun-synchronous, polar orbits that produce global coverage every two days with a nadir spatial resolution of 1.1 km^2.

Ocean color satellite instruments provide estimates of remote-sensing reflectances ($R_{rs}(\lambda)$, sr^{-1}) after atmospheric correction. Standard NASA ocean color data processing uses globally tuned algorithms to relate $R_{rs}(\lambda)$ to secondary geophysical data products, such as C_a, many of which remain empirical in form and function (McClain, 2009). The standard C_a algorithms for SeaWiFS and MODISA (OC4 and OC3M, respectively; O'Reilly et al., 1998) relate ratios of blue-to-green $R_{rs}(\lambda)$ to C_a based on statistical relationships observed using a global in situ data set (Werdell and Bailey, 2005). In some instances, the accuracy of those estimates has been found to underperform when assessed at regional scales. In high-latitude oceans, lower pigment specific spectral absorption coefficients have been invoked to explain the underestimation of C_a by global ocean color algorithms (Cota et al., 2003; Dierssen and Smith, 2000; Mitchell, 1992; Mitchell and Holm-Hansen, 1991). In the Arctic, those biases have been found to be non-uniform throughout the basin, but with consistent patterns of under and over estimation circumscribed to specific regions. In the Labrador Sea, the OC4 algorithm was found to underestimate C_a by 50% over most of its dynamic range (Cota et al., 2003), while in the western Arctic Ocean (i.e., Beaufort and Chukchi seas) and the Arctic region of the Atlantic, the bias has been consistently towards overestimation (Ben Mustapha et al., 2012; Matsuoka et al., 2007; Stramska et al., 2003; Wang and Cota, 2003). Atypically high absorption by chromophoric dissolved organic matter (CDOM) from river inputs to this Arctic region has been suggested as the main cause for C_a overestimation from satellite radiometry (Brunelle et al., 2012; Matsuoka et al., 2007). Attempts at developing regionally tuned C_a for the Arctic (Cota et al., 2004; Wang and Cota, 2003) have had mixed successes (Ben Mustapha et al., 2012; Matsuoka et al., 2007).

Regional empirical C_a algorithms for the Arctic, and other ocean regions, are based on linear corrections built upon the global, empirically-derived algorithms, and thus rest upon the same bio-optical assumption that the IOPs of natural waters covary with the concentration of C_a (Gordon and Morel, 1983; Siegel et al., 2002, 2005). All ocean basins deviate from this ideal and are to some extent optically different, and those differences are linked to systematic variability in community structure and biogeochemical function (Loisel et al., 2010; Sauer et al., 2012; Szeto et al., 2011). Semi-analytical algorithms (SAAs) provide an alternative to the band ratio approaches described above (IOCCG, 2006; Werdell et al., 2013a). SAAs use combinations of empiricism and radiative transfer theory to simultaneously estimate concentrations of IOPs for C_a, non-algal particles, and CDOM, thereby eliminating the need for the bio-optical assumption and conceptually improving the performance of C_a retrievals, particularly in areas where historically traditional approaches have lagged. Initial assessments of IOP time-series from SAAs in the Arctic Ocean have shown potential for improving remote sensing C_a retrievals in the Arctic (Bélanger et al., 2007; Ben Mustapha et al., 2012). Only very recently have the broad datasets necessary for this task been assembled as the direct result of programs such as ICESCAPE, Malina, and Takuvik (Antoine et al., 2013; Matsuoka et al., 2013b; Zheng et al., in press).

Our contributions to this emerging body of work on ocean color remote-sensing of the Arctic are twofold and all within the context of defining new requirements for advanced satellite instruments with increased spectral resolution (e.g., the NASA Pre-Aerosols, Clouds, and ocean Ecosystems (PACE) mission scheduled for launch in 2020 (PACE Mission Science Definition Team, 2012)). First, we evaluated the quality of standard MODISA ocean color data records in the western Arctic Ocean using in situ data collected during the ICESCAPE campaigns as ground truth. Doing so assessed the quality of standard (current operational) MODISA-derived products for use in Arctic climate studies and reiterated the need for advanced algorithm approaches that simultaneously account for phytoplankton, non-algal particles, and CDOM (Bélanger et al., 2007; Ben Mustapha et al., 2012). Second, we explored the advantages of incorporating additional wavelengths into semi-analytical inversion algorithms. Doing so reinforced the potential benefits of advanced instrument systems with increased spectral resolution for Arctic studies. We acknowledge that ICESCAPE provides only a temporally-limited snapshot of Arctic biogeochemistry and MODISA was only one of several operational satellite missions during the field campaigns. Given the aforementioned goals, however – and the complementary studies in this special issue that benefit from an evaluation of MODISA data records – our highly focused results contribute to the growing foundation of Arctic remote sensing research. We chose MODISA for our analyses since it was best performing NASA ocean color sensor operational at the time of both ICESCAPE field campaigns (Franz et al., 2008).

2. Material and methods

2.1. In situ data collection

Field observations (Fig. 1) were conducted during two ICESCAPE field campaigns, from June 15 to July 22, 2010, and from June 25 to July 29, 2011, onboard the US Coast Guard Cutter *Healy*. The field observations in this study were carried out from the Arctic Survey Boat (ASB), which was deployed off the *Healy* almost daily when sea and ice conditions permitted. The ASB is a 10 m aluminum landing craft that provided a suitable platform for making accurate measurements of the underwater light field away from the water disturbed by the cutter and closer to the ice edges.

Two replicate surface water samples for analysis of phytoplankton pigments, POC, and spectral absorption by particles ($a_p(\lambda)$; m^{-1}) were collected using clean, 10 L polyethylene containers at each station. Surface samples for analysis of CDOM absorption ($a_g(\lambda)$; m^{-1}) were collected using clean, combusted (450 °C, 4 h) 500 mL amber glass

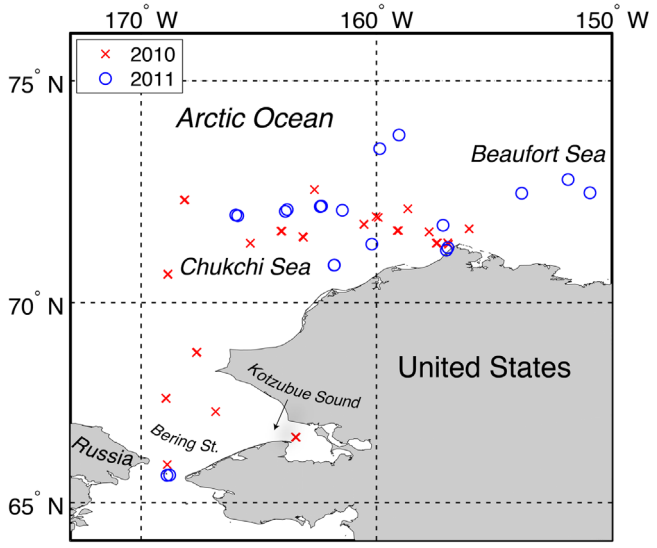

Fig. 1. Map of the area of study. Symbols denote Arctic Survey Boat (ASB) stations carried out during the 2010 and 2011 ICESCAPE campaigns.

bottles. Determinations of C_a, other photosynthetic and accessory pigments, POC, and $a_p(\lambda)$, were performed on material retained on 25 mm, 0.7 mm pore size Whatman GF/F filters under low vacuum (<50 kPa). Phytoplankton pigments were determined using high performance liquid chromatography (HPLC) following the procedures of Van Heukelem and Thomas (2001), as further described in Hooker et al. (2005).

The optical density of particulate matter ($OD_f(\lambda)$; unitless) was measured on a Perkin Elmer Lambda 35 spectrophotometer using a spectral range of 300–800 nm. The clearance area of the filter (A_f; m^2) was measured with calipers. To measure the $OD_f(\lambda)$ of non-pigmented materials ($a_d(\lambda)$; m^{-1}), the filters were extracted using 95% methanol and rescanned (Kishino et al., 1985). The total particulate and de-pigmented absorption coefficients were calculated by

$$a_{p/d}(\lambda) = 2.303 * (OD_{f,p/d}(\lambda) - OD_{bs}(\lambda) - OD_{null}(\lambda))/(\beta l) \quad (1)$$

where β is the pathlength amplification correction set to 2 (unitless), and $OD_{bs}(\lambda)$ is the optical density of the blank GF/F filter. The path length, l (m), is given by

$$l = V_f/A_f \quad (2)$$

where V_f (m^3) is the filtered volume (Mitchell et al., 2003; Roesler, 1998). The $OD_f(\lambda)$ of $a_p(750)$ and $a_d(750)$ were assumed to be zero (OD_{null}). The phytoplankton absorption coefficient, $a_{ph}(\lambda)$, is then given by

$$a_{ph}(\lambda) = a_p(\lambda) - a_d(\lambda) \quad (3)$$

Samples for determination of $a_g(\lambda)$ were GF/F filtered at sea and stored at 8 °C in clean, combusted 250 mL amber-colored glass bottles for delivery to NASA Goddard Space Flight Center for analysis. Prior to $a_g(\lambda)$ determination, samples were re-filtered (pre-rinsed 0.22 μm membrane filters) in the laboratory and absorbance spectra ($A(\lambda)$; unitless) were measured against a Milli-Q pure water reference on a 2 m-pathlength, liquid core waveguide absorption cell coupled to a Tidas I fiber optic spectrometer (WPI Inc.; Miller et al., 2002). Measured absorbances were corrected for the difference in refractive indices between the reference and the salt-containing samples. A linear correction was derived from the absorbances measured on NaCl solutions of known salinity against a pure water reference. The corresponding spectral absorbance correction for a given salinity was subtracted from the observed sample spectrum. The spectral absorption coefficients were obtained by

$$a_g(\lambda) = 2.303 A(\lambda)/L \quad (4)$$

where L is the pathlength in meters. Absorbance data were corrected for baseline offsets by subtracting the average absorbance value between 690 and 700 nm. The spectral absorption coefficient of dissolved plus non-algal detrital material, $a_{dg}(\lambda)$, is then given by

$$a_{dg}(l) = a_g(\lambda) + a_d(\lambda) \quad (5)$$

Currently, the contributions of $a_d(\lambda)$ and $a_g(\lambda)$ cannot be separated in the satellite algorithm paradigm as they maintain the same spectral shapes (IOCCG, 2006).

POC was determined on a Perkin Elmer 2400 elemental analyzer, following the protocols of the Joint Global Ocean Flux Study (Knap et al., 1996). The instrument was calibrated using acetanilide (C_8H_9NO) standards weighed at a precision of 0.001 mg. For quality assessment, National Institute of Standards and Technology (NIST) reference material (Buffalo River Sediment, NIST 8704) was analyzed along with samples. The root mean squared percentage error (RMSPE) for reference material determinations were 9.7% and 4.4%, for the 2010 and 2011samples, respectively.

The radiometric quantities upwelling radiance ($L_u(\lambda)$; $\mu W\,cm^{-2}\,nm^{-1}\,sr^{-1}$) and downwelling irradiance ($E_d(\lambda)$; $\mu W\,cm^{-2}\,nm^{-1}$) were measured at 19 spectral bands between 300 and 900 nm using hand-deployed C-OPS and SuBOPS submersible profiling radiometers (Biospherical Instruments, Inc.; Hooker et al., 2010; Morrow et al., 2010), respectively, during the 2010 and 2011 campaigns following NASA Ocean Optics Protocols (Mueller and Austin, 1995). A radiometer to measure surface solar irradiance ($E_s(\lambda)$; $\mu W\,cm^{-2}\,nm^{-1}$) in corresponding spectral bands was mounted atop a telescoping mast with a clear view of the sky on board the ASB (Hooker, 2010). Remote sensing reflectances ($R_{rs}(\lambda)$; sr^{-1}) and spectral diffuse attenuation coefficients for $E_d(\lambda)$($K_d(\lambda)$; m^{-1}) were calculated from the radiometric profiles via the methods described in Werdell and Bailey (2005), and references therein. A linear exponential fit was applied to radiance and irradiance profiles to calculate the spectral diffuse attenuation coefficients. Those coefficients were used to propagate radiances and irradiances to below-surface values, which were then transmitted across the air-sea interface (Mueller and Austin, 1995). Quality control and assurance applied to these apparent optical properties (AOPs) is further described in Werdell and Bailey (2005).

Approximately 90% of what a satellite ocean color instrument measures includes weighted contributions from all water column constituents more shallow than the e-folding depth for $K_d(\lambda)$ (Gordon and McCluney, 1975).While the optical weighting of biogeochemical parameters remains desirable for ocean color data product validation activities, this could not be achieved using our data set since only surface discrete water samples were collected (e.g., Zaneveld et al., 2005). We expect this inability to optically weight our C_a, POC, and IOP samples to impart only minor variability into our results, as the majority of our stations maintained e-folding depths for $K_d(443)$ between 5 and 10 m.

2.2. Satellite data

MODISA Level 2 data records that encompassed the two ICESCAPE campaigns were acquired from the NASA Ocean Biology Processing Group (OBPG: http://oceancolor.gsfc.nasa.gov). Using these data records, satellite-to-in situ match-ups for MODISA were generated using the operational OBPG validation infrastructure (http://seabass.gsfc.nasa.gov/seabasscgi/search.cgi). Satellite data processing and quality assurance for these match-ups followed Bailey and Werdell (2006). Specifically: (a) temporal coincidence was defined as ± 3 h; (b) satellite values were the filtered mean of all

unmasked pixels in a 5×5 box centered on the in situ target; and (c) satellite values were excluded when the median coefficient of variation for unflagged pixels within the box exceeded 0.15. These temporal and spatial thresholds were developed for the open ocean and may not be ideal for a dynamic region such as the western Arctic, where adjacency effects along sea ice margins and pixel contamination by sea ice are known additional sources of error (Bélanger et al., 2007). However, reducing the window of temporal coincidence to ± 1 h and the satellite box to 3×3 pixels did not change the number of match-ups or significantly alter our results. Regression statistics were calculated using Type II methods; the caption of Table 1 provides definitions and calculation methods for the statistics. Finally, MODISA Level 3 composites for the duration each ICESCAPE campaign at 2 km spatial resolution were generated from the Level 2 data records using OBPG binning software (l2bin and l3gen). Standard Level 3 masks were used, as described in Franz et al. (2005).

2.3. Bio-optical algorithms

Modeled estimates of C_a, POC, and spectral IOPs were generated using both the in situ and MODISA $R_{rs}(\lambda)$. The following algorithms and data products were used:

Table 1
Type II regression statistics for modeled geophysical parameters calculated using in situ R_{rs} vs. in situ measured parameters. N is sample size; r^2 is the coefficient of determination; slope ($\pm$SE) is the regression slope plus/minus its standard error. RMSE is the residual mean square error of the regression. Ratio is the median ratio calculated as median (model/in situ). The r^2, Slope, and RMSE were calculated using log-transformed data for C_a, a_{ph}, and a_{dg}. C_a is from OC3M. POC is from Stramski (2008). The absorption coefficients are from the GIOP algorithm. Six MODISA wavelengths were used as input to GIOP (412, 443, 488, 531, 547, and 667 nm).

	N	r^2	Slope ($\pm$SE)	RMSE	Ratio
C_a (OC3M)	33	0.62	0.72 (0.08)	0.295	3.05
C_a (GIOP)	32	0.72	0.73 (0.07)	0.245	1.56
POC	41	0.63	1.04 (0.11)	147.97	1.08
$a_{ph}(443)$	33	0.85	1.18 (0.08)	0.202	1.64
$a_{dg}(443)$	30	0.91	1.05 (0.11)	0.082	0.77

- C_a from O'Reilly et al. (1998; OC3M);
- C_a, $a_{ph}(\lambda)$, and $a_{dg}(\lambda)$ from Werdell et al. (2013a, 2013b; GIOP).
- POC from Stramski et al. (2008; hereafter Stramski POC).

Note these are all data products that NASA produces operationally for the ocean color satellites for which they maintain responsibility. Both OC3M and the Stramski POC algorithm use blue-to-green ratios of $R_{rs}(\lambda)$ as input into empirical expressions. OC3M uses the greater of $R_{rs}(443)/R_{rs}(547)$ and $R_{rs}(488)/R_{rs}(547)$, while the Stramski POC algorithm uses $R_{rs}(488)/R_{rs}(547)$. The sequencing band ratios of OC3M are hereafter referred to as a maximum band ratio (MBR; O'Reilly et al., 1998). Note that the current OBPG version of OC3M includes the modifications presented in http://oceancolor.gsfc.nasa.gov/ANALYSIS/ocv6/.

In contrast to the latter algorithms, Generalized Inherent Optical Property model (GIOP) is a spectral matching inversion model (i.e., SAA) that uses nonlinear least squares methods to solve for three eigenvalues ($a_{ph}(443)$, $a_{dg}(443)$, and the spectral backscattering coefficient for particles ($b_{bp}(\lambda)$; m^{-1}) at 443 nm) using predefined eigenvectors (spectral shapes for the three components). GIOP produces estimates of C_a through the relationship $a_{ph}(443)=0.055\ C_a$, where 0.055 represents the C_a-specific absorption coefficient ($m^2\ mg^{-1}$) at 443 nm. We used the default configuration of GIOP; Werdell et al. (2013a) modified following Werdell et al. (2013b); Werdell et al. (2013a) provide additional details on the operation and limitations of GIOP. GIOP was applied twice to in situ $R_{rs}(\lambda)$ – first using only six MODISA wavelengths (412, 443, 488, 531, 547, and 667 nm) to mimic the satellite application of this algorithm, and then using 11 wavelengths (adding 395, 465, 510, 560, and 625 nm to the standard MODISA suite).

We acknowledge that alternative SAAs exist, including regionally tuned versions [e.g., the Garver–Siegel–Maritorena (GSM) approach of Maritorena et al. (2002), the Quasi-Analytical Algorithm (QAA) of Lee et al. (2002), and their modified versions in Ben Mustapha et al. (2012) and Bélanger et al. (2007), respectively]. An algorithm inter-comparison exercise, however, exceeded the scope

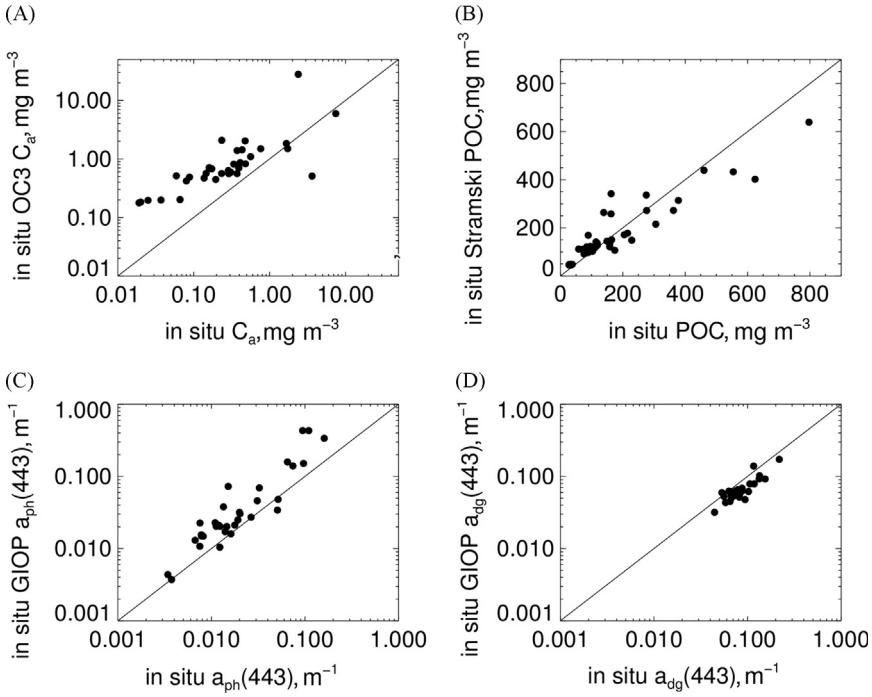

Fig. 2. OC3M estimated C_a (A), Stramski POC (B), GIOP $a_{ph}(443)$ (C), and GIOP $a_{dg}(443)$ (D) using in situ $R_{rs}(\lambda)$, versus in situ measured values. Supporting Type II regression statistics are provided in Table 1.

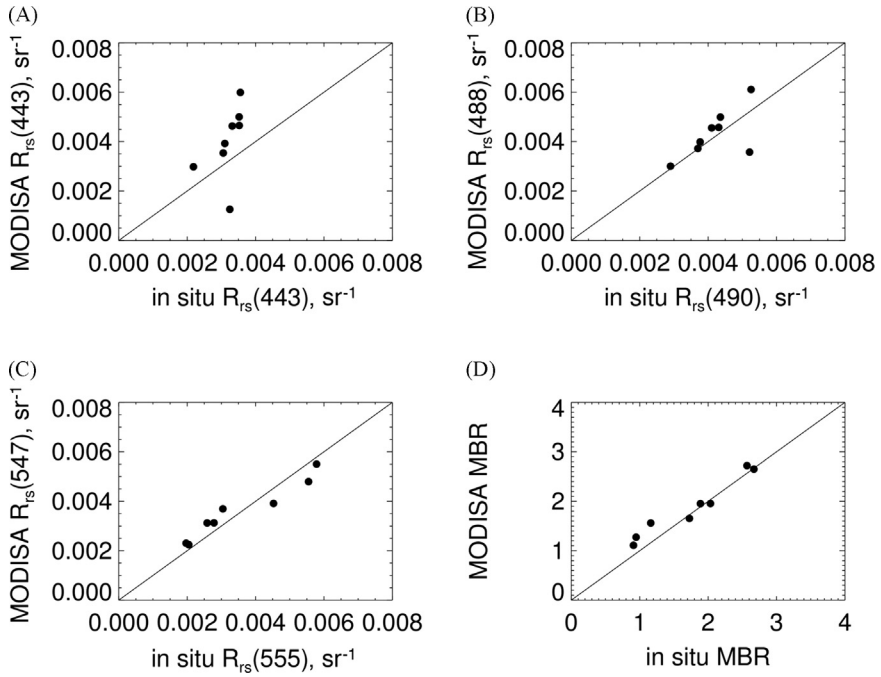

Fig. 3. MODISA versus in situ R_{rs} at 443 (A), 488 (B) and 547 (C) nm. The maximum band ratio (MBR), calculated as max (R_{rs}443 > R_{rs}488)/R_{rs}547, is shown in (D). The MBR is used as input into the OC3M algorithm. Type II regression statistics are presented in Table 2.

Table 2
Type II regression statistics for MODISA products vs. in situ measured parameters. See Table 1 caption for additional details.

	N	r^2	Slope (± SE)	RMSE	Ratio
R_{rs}(412)	7	0.15	4.29 (2.11)	0.0013	1.52
R_{rs}(443)	7	0.73	2.06 (0.50)	0.0006	1.37
R_{rs}(488)	7	0.98	1.37 (0.10)	0.0002	1.06
R_{rs}(531)	7	0.96	0.97 (0.08)	0.0002	1.06
R_{rs}(547)	7	0.92	0.79 (0.10)	0.0003	1.12
R_{rs}(667)	7	0.94	0.87 (0.09)	0.00001	1.07
MBR	7	0.94	0.88 (0.10)	0.160	1.03
POC	13	0.93	0.55 (0.05)	35.15	0.92
C_a (OC3M)	10	0.64	0.37 (0.10)	0.177	3.95
C_a (GIOP)	10	0.65	0.44 (0.11)	0.205	3.62
a_{ph}(443)	12	0.64	0.92 (0.19)	0.260	2.22
a_{dg}(443)	10	0.44	−0.74 (0.21)	0.119	0.43

of this manuscript and did not substantially contribute to our stated goals of comparing empirical and SAA approaches and exploring expanded spectral resolutions. Furthermore, previous studies have shown GIOP to perform equivalently to or better than GSM and QAA on global scales (Brewin et al., 2013; Werdell et al., 2013a, 2013b). We recommend that future studies continue to explore regional parameterizations (Bélanger et al., 2007, Ben Mustapha et al., 2012) and ensemble approaches for applying SAAs [such as the optical water type method of Moore et al. (2009) or the iterative method of Brando et al. (2012)] with particular emphases on exploiting increased spectral resolution.

3. Results

The direct comparison of modeled and ground-truth (in this case, in situ) values provided a straightforward mechanism for assessing the accuracy of the MODISA bio-optical algorithms. OC3M C_a derived using in situ $R_{rs}(\lambda)$ was positively biased relative to in situ C_a, with a model-to-in situ ratio of 3.05 (Table 1). This was particularly true for values below 1 mg m^{-3}, which ultimately led to a depressed regression slope of 0.72 (Fig. 2a). When only considering $C_a \leq 1$ and 0.2 mg m^{-3}, the ratios rose to 3.37 and 5.25 and the slopes fell to 0.66 and 0.64, respectively. GIOP C_a showed significantly reduced bias relative to that from OC3M, as the ratio for all C_a fell to 1.56, but maintained a similar regression slope of 0.73. Stramski POC calculated with in situ R_{rs} performed statistically better than the C_a algorithms. As demonstrated by its slope of 1.04 and ratio of 1.08, the Stramski POC showed no clear bias relative to in situ measurements over its full dynamic range (Fig. 2b). The six-wavelength GIOP run provided reasonable estimates of a_{ph}(443) and a_{dg}(443) with slopes slightly above unity, but with positively and negatively biased model-to-in situ ratios of 1.64 and 0.77, respectively (Fig. 2c, d). GIOP showed significant improvement over OC3M with regards to estimating the presence of phytoplankton over its full dynamic range. The r^2, regression slope, and RMSE for OC3M C_a improved from 0.62, 0.72, and 0.295, respectively, to 0.85, 1.18, and 0.202 for GIOP a_{ph}(443). GIOP less variably described phytoplankton signatures with $a_{ph}(\lambda)$ than with C_a, most likely due to the inability of the fixed value of a^*_{ph}(443) (=0.055 m^2 mg^{-1}) to accurately represent phytoplankton physiological conditions at all times. For context, the mean a^*_{ph}(443) for our two field campaign data set was 0.054 (± 0.025) m^2 mg^{-1}.

MODISA-versus-in situ Level 2 $R_{rs}(\lambda)$ match-ups showed better agreement in green wavelengths than in blue wavelengths, with MODISA values exceeding in situ values at wavelengths less than 488 nm (Fig. 3a–c, Table 2). This overestimation was spectrally dependent with regression slopes and satellite-to-in situ ratios that sequentially fell from 4.29 and 1.52, respectively, to 0.97 and 1.06 from R_{rs}(412) to R_{rs}(531). Nevertheless, the MBR agreement was very good, with a satellite-to-in situ ratio of 1.03 (Fig. 3d). While the brightening of MODISA $R_{rs}(\lambda)$ had spectral dependence, the MBR predominantly used R_{rs}(488) and R_{rs}(547) (also the input to the Stramski POC algorithm), which had comparable satellite-to-in situ ratios of 1.06 and 1.12, respectively. We expect that this Rayleigh-like brightening of blue wavelengths resulted from adjacency effects imposed, for example, by the nearby presence of ice edges (Bélanger et al., 2007; Perovich, 1996; Warren, 1982;

Warren et al., 2006) in combination with imperfect atmospheric correction due to the elevated solar and sensor geometries that occur at high latitudes. Furthermore, elevated turbidity (e.g., when C_a exceeds 1 or 2 mg m^{-3}) triggers a bio-optical model within the atmospheric correction process to account for non-negligible near-infrared $R_{rs}(\lambda)$ (Bailey et al., 2010). The applicability of this bio-optical model to Arctic waters requires further evaluation.

The patterns of modeled-versus-measured C_a, POC, and IOPs for MODISA $R_{rs}(\lambda)$ were similar to those modeled using in situ R_{rs} (λ), which was not unexpected for OC3M and Stramski POC algorithms given the similarities in the satellite and in situ $R_{rs}(\lambda)$ at 488 and 547 nm (Table 2). OC3M C_a from MODISA versus HPLC C_a yielded r^2, regression slope, and ratios of 0.64, 0.37, and 3.95, respectively, compared to 0.62, 0.72, and 3.05 for OC3M C_a from in situ $R_{rs}(\lambda)$. Both in situ- and MODISA-derived C_a showed clear elevated biases at values below 1 mg m^{-3} (Fig. 4a). When only considering $C_a \leq 1$ and 0.2 mg m^{-3}, the ratios rose to 4.02 and 4.57, respectively. Qualitatively, the MODISA-derived Stramski POC achieved as good agreement with in situ measurements as did the estimates obtained with in situ $R_{rs}(\lambda)$ (Fig. 4b), however its slope and ratio fell to 0.55 and 0.92. Despite the spectral brightening of blue MODIS $R_{rs}(\lambda)$, $a_{ph}(443)$ and $a_{dg}(443)$ from GIOP also attained comparable metrics to estimates obtained using GIOP with in situ radiometry at MODISA wavelengths (Fig. 4c, d). Both in situ- and MODISA-derived IOPs showed similar biases in comparison with field measurements – specifically, ratios of 1.64 and 2.22 for $a_{ph}(443)$, and 0.77 and 0.43 for $a_{dg}(443)$. Note that in all cases, the number of in situ samples (Table 1) exceeded those from MODISA (Table 2) by approximately three-fold due to the small number of satellite-in situ matchups attained during both campaigns.

MODISA Level 3 composites for both ICESCAPE campaigns reiterated that C_a from an empirical approach (OC3M) consistently exceeds that from a semi-analytical approach (GIOP) in the western Arctic (Figs. 5a, b and 6a, b). For both 2010 and 2011, regions where such differences were most qualitatively obvious corresponded to regions with the highest CDOM (as inferred via $a_{dg}(443)$). For example, consider the areas around the Bering Strait and near the receding ice edge at the north end of each scene, as opposed to those near the Alaskan coast and Kotzubue Sound on the Level 3 imagery (Figs. 5 and 6). Around the former, particularly in 2010, GIOP reported low $a_{dg}(443)$ and prominent features of high C_a captured by both OC3M and GIOP. On the other hand, along the AK coast, particularly in Kotzbue Sound, GIOP $a_{dg}(443)$ and OC3M C_a were both high, whereas the magnitude of GIOP C_a was much reduced. These examples imply that either elevated $a_{dg}(443)$ or $a_{ph}(443)$ triggered OC3M to report elevated C_a, which is consistent with previous findings that OC3M and OC4 mistake elevated CDOM as elevated C_a (Ben Mustapha et al., 2012; Matsuoka et al., 2007). Maps of unbiased percent difference (UPD; see Fig. 7 for its calculation) between OC3M and GIOP C_a showed that the regions of least difference between those estimates, during both campaigns, were located towards the receding ice edge, away from the coast, and in the Bering Strait where those high C_a features occurred. These two example regions (i.e., Bering St., ice edge vs. AK coast, Kotzbue sound) corresponded to the minimal and maximal UPDs in the Level 3 composites. MODISA data along the USCGC *Healy* cruise tracks during the ICESCAPE campaigns further underscore the overestimation of C_a by OC3M in the regions of highest CDOM (Fig. 8). There is marked coherence between the UPD between OC3M and GIOP C_a and $a_{dg}(443)$ along the cruise tracks for both campaigns. The UPD between those estimates trended towards null as $a_{dg}(443)$ decreased below values of 0.02 m^{-1}, and reached values above 100% as $a_{dg}(443)$ 0.10 m^{-1}.

4. Discussion

Our observations of positively biased OC3M C_a relative to coincident in situ measurements are consistent with previous studies that have evaluated the performance of empirical, globally tuned ocean color algorithms in the Arctic Ocean (Ben Mustapha et al., 2012; Cota et al., 2004; Stramska et al., 2003). These biases were realized for both the MODISA and in situ $R_{rs}(\lambda)$, which

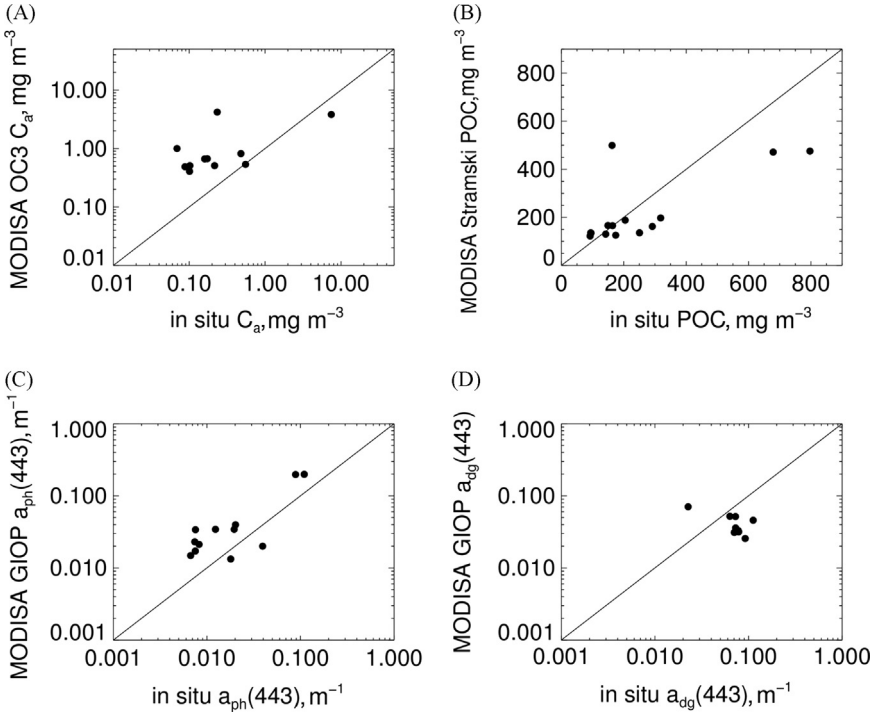

Fig. 4. MODISA C_a (A) and POC (B); GIOP $a_{ph}(443)$ (C) and $a_{dg}(443)$ (D) using MODISA $R_{rs}(\lambda)$ versus in situ measured values. Supporting Type II regression statistics are provided in Table 2.

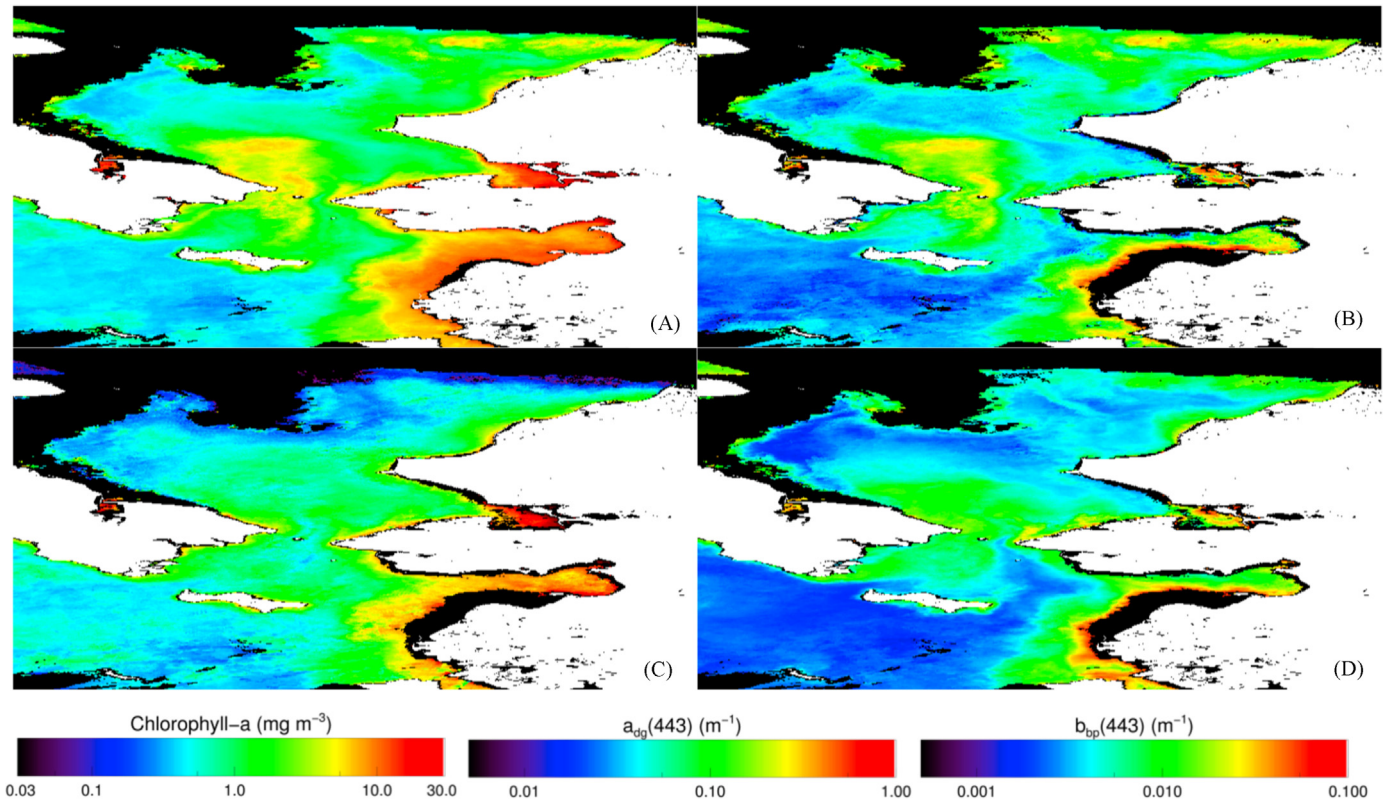

Fig. 5. Level 3 MODISA composites for the region of study during ICESCAPE 2010: (A) OC3M C_a; (B) GIOP C_a; (C) GIOP $a_{dg}(443)$; and (D) $b_{bp}(443)$.

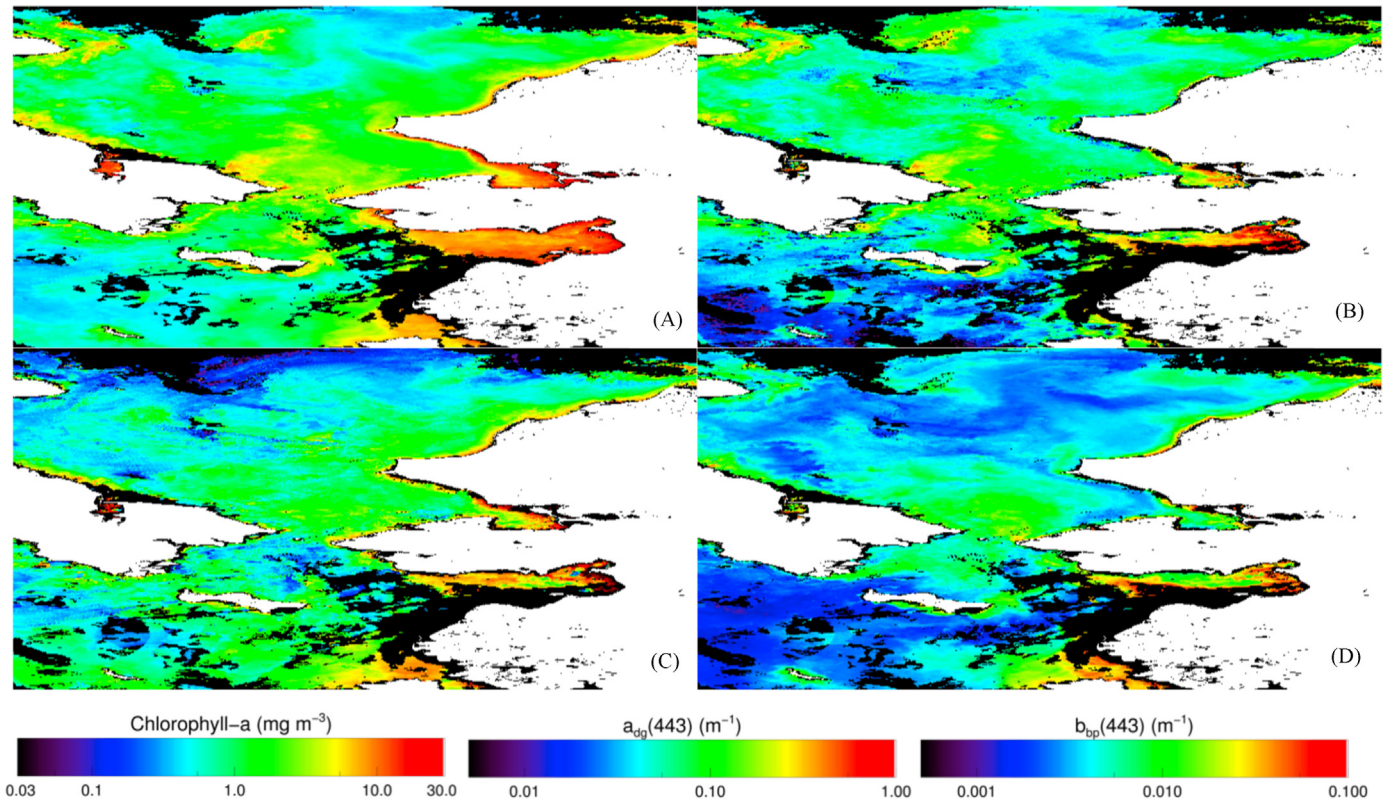

Fig. 6. Level 3 MODISA composites for the region of study during ICESCAPE 2011: (A) OC3M C_a; (B) GIOP C_a; (C) GIOP $a_{dg}(443)$; and (D) $b_{bp}(443)$.

implies the source of the bias was the bio-optical algorithm and not by the observed radiometry (Tables 1 and 2, Figs. 2 and 4). In general, the relationship between MODISA and in situ MBR versus in situ C_a from ICESCAPE fell well below the global relationship employed by OC3M, which was derived using the NASA bio-Optical Marine Algorithm data set (NOMAD; Werdell and Bailey,

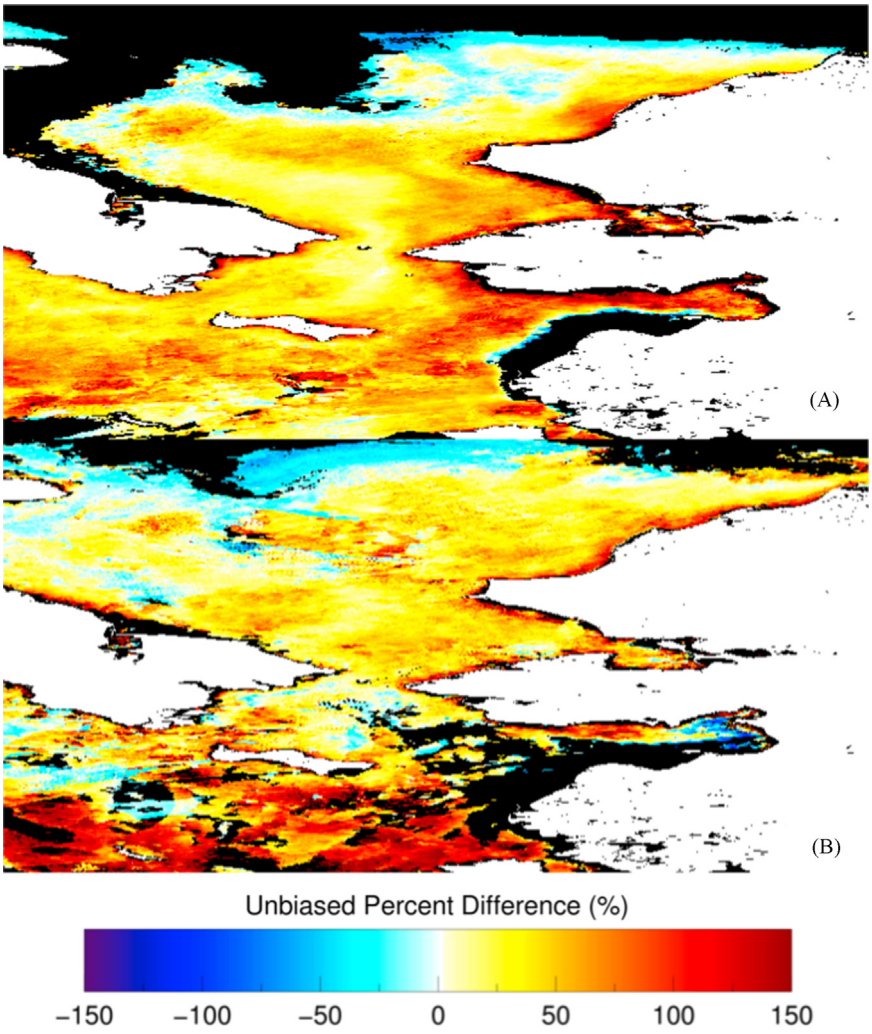

Fig. 7. Level 3 MODISA composites for the unbiased percent difference (UPD) between OC3M and GIOP C_a, for the ICESCAPE campaigns in (A) 2010, and (B) 2011. UPD was calculated as 200% * (OC3M-GIOP)/(OC3M+GIOP). Black denotes pixels flagged for ice, clouds, or sediments.

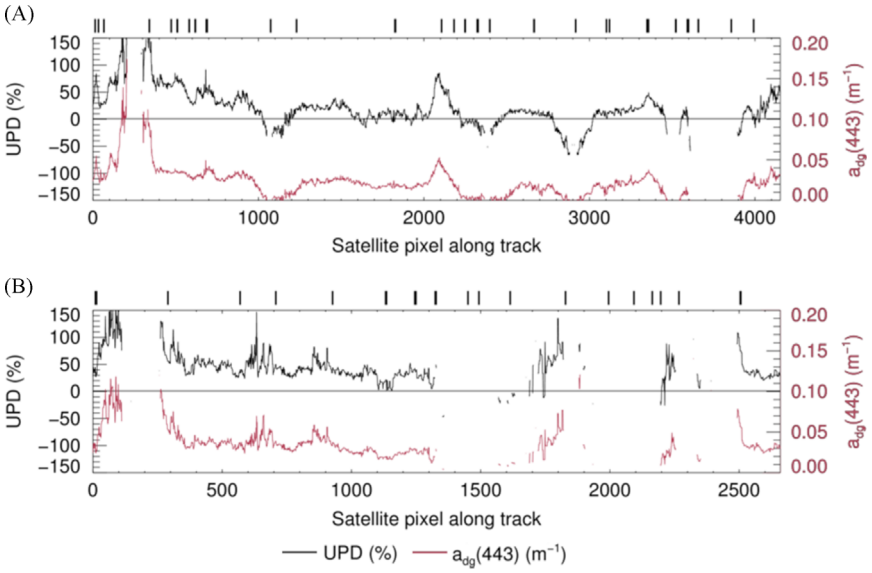

Fig. 8. Unbiased percent difference (UPD) between OC3M and GIOP C_a, and $a_{dg}(443)$, for MODISA pixels collected along the track of the USCGC *Healy* during the ICESCAPE 2010 (A), and 2011 (B) campaigns. The right *y*-axis show $a_{dg}(443)$, which is shown in red in both panels. Tick marks above each plot indicate the locations along track where in situ ASB observations were conducted.

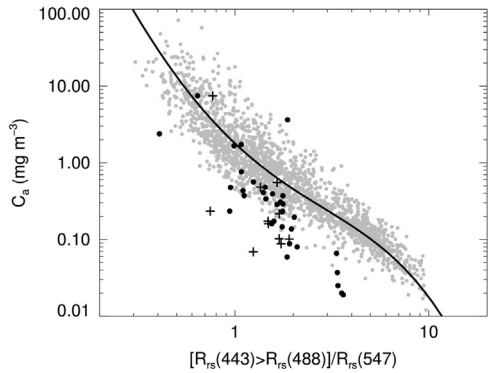

Fig. 9. In situ HPLC C_a versus Maximum Band Ratio (MBR) from in situ radiometry (black circles), and from MODISA (crosses), for observations collected during the ICESCAPEs campaigns. The gray points are the observations in the NASA Bio-Optical Marine Algorithm Data Set (NOMAD; Werdell and Bailey, 2005) used to derive the MODISA OC3M algorithm (solid line).

Table 3
Type II regression statistics for IOPs from GIOP calculated using in situ $R_{rs}(\lambda)$ at eleven wavelengths (adding 395, 465, 510, 560, and 625 nm to the suite of MODISA λ) vs. in situ measured parameters. See Table 1 caption for additional details.

	N	r^2	Slope ($\pm$ SE)	RMSE	Ratio
C_a (GIOP)	32	0.69	0.65 (0.07)	0.232	1.59
$a_{ph}(443)$	33	0.87	1.16 (0.08)	0.184	1.38
$a_{dg}(443)$	30	0.92	1.03 (0.05)	0.077	1.33

2005) (Fig. 9). These depressed blue-to-green ratios of $R_{rs}(\lambda)$ (relative to what has been observed on average globally) resulted in positively biased C_a in the western Arctic. This geographic region appears to be bio-optically unique, as the bulk of the ICESCAPE observations occupy a region of the C_a-MBR space that maintains little or no overlap with the extent of the globally-distributed NOMAD observations, particularly at $C_a < 0.5$ mg m^{-3}. Furthermore, at the very low end of the dynamic range of OC3M (i.e., $0.01 < C_a < 0.1$ mg m^{-3}), the measurements from ICESCAPE share no commonality with any other major ocean basin (see Fig. 1 in Szeto et al., 2011). If the bio-optical signatures we observed in the western Arctic Ocean waters are typical at basin-wide scales, attempts to derive pan-Arctic satellite ocean color-based carbon stock assessments could render potentially large overestimations.

In contrast, the satisfactory performance of the Stramski POC algorithm (Tables 1 and 2, Figs. 2 and 4) suggests that the datasets used to craft the empirical relationships for that algorithm better represent high latitude oceans. The fundamental relationships behind the bio-optical linkage between suspended particulate stocks (which include chlorophyll-bearing, live phytoplankton, heterotrophic organisms, as well as detrital particulates) are less variable due to a detrital portion that is more homogenous in its bio-optical signature. Particle concentration is expected to covary well with the bulk scattering properties of seawater (e.g., $b_{bp}(\lambda)$), especially in the region of the spectrum where particles absorb weakly (Stramska and Stramski, 2005, and references therein), which incidentally are the regions of the spectrum (i.e., >500 nm) where a_g is less important. The authors of the Stramski POC algorithm noted that "[their] proposed band ratio algorithms have similar regression coefficients to those previously determined from selected historical data sets that included 205 data pairs of POC and reflectance measured in several oceanic regions" (Stramski et al., 2008). Moreover, the work that established the underlying bio-optical relationships between POC stocks and water-leaving radiances was derived from a large fraction of field observations acquired in the Southern Ocean and the north polar Atlantic (Stramska and Stramski, 2005; Stramski et al., 1999).

In the western Arctic Ocean, the OC3M algorithm appears to attribute CDOM absorption, $a_g(\lambda)$, to phytoplankton absorption, $a_{ph}(\lambda)$ (Matsuoka et al., 2007). Conceptually, excess $a_g(\lambda)$ (relative to what would be derivative of only phytoplankton) produces lower MBRs that result in overestimates of C_a (Fig. 9). In the western Arctic, we do not expect $a_{dg}(\lambda)$ to covary with C_a as it does in lower latitude and oligotrophic oceans (Siegel et al., 2002, 2005). High levels of CDOM in Arctic Ocean waters have been widely documented (e.g., Brunelle et al., 2012; Granskog et al., 2012; Guéguen et al., 2005; Matsuoka et al., 2013a, 2011, 2007; Pegau, 2002; Stedmon et al., 2011). The basin as a whole receives the largest dissolved organic carbon input (and hence CDOM input) from rivers, relative to its size, than any other ocean basin (Rachold et al., 2004). In the western Arctic Ocean, $a_g(\lambda)$ has been reported as more than 50% of the total non-water absorption at all visible wavelengths, and up to 75% at 443 nm (Brunelle et al., 2012; Matsuoka et al., 2007).

GIOP effectively estimated both phytoplankton and CDOM absorption (Figs. 2 and 4). Like most SAAs, GIOP does not assume covariance between $a_{dg}(\lambda)$ and C_a. The quality of the absorption estimates and the demonstrated deficiencies in OC3M C_a suggest to a first order that SAAs provide more reliable data records for western Arctic studies than do existing empirical methods. GIOP provided less variable estimates of $a_{ph}(443)$ ($r^2=0.85$; Table 1) than of C_a ($r^2=0.72$; Table 1). In principle, this suggests that the spectral shape of the C_a-specific absorption coefficient employed by GIOP (from Bricaud et al., 1998) is adequate for the western Arctic, but that its magnitude ($a^*_{ph}(443)=0.055$ m^2 mg^{-1}) is insufficient to unequivocally relate absorption to C_a at all times. The mean observed $a^*_{ph}(443)$ for our two field campaigns matched the GIOP default (0.054 ± 0.025 m^2 mg^{-1}), but ranged from 0.009 to 0.102 m^2 mg^{-1}. Studies that have measured $a^*_{ph}(\lambda)$ in Arctic waters have found strong seasonality caused by changes in "pigment packaging" associated with the extreme seasonal variation in light availability (Brunelle et al., 2012; Matsuoka et al., 2011). Well-established interdependencies between $a^*_{ph}(\lambda)$ and phytoplankton community indices (e.g., C_a, dominant cell size) at lower latitudes (Ciotti et al., 2002), might be upended in Arctic waters by the strong seasonality and its effect on phytoplankton physiology (Brunelle et al., 2012).

In practice, future studies with interest in Arctic phytoplankton dynamics and production might benefit from evaluating absorption spectra in lieu of C_a abundances. Alternatively, when stocks and abundances are required, regional relationships between $a_{ph}(\lambda)$ and C_a could be developed for application to the GIOP-derived $a_{ph}(\lambda)$ following, for example, the approach presented in Werdell et al. (2013c). A sufficient in situ data set exists from ICESCAPE such that regional statistical relationships between $a_{ph}(443)$ and C_a can be developed (e.g., Bricaud et al., 1998; Werdell et al., 2013c). Our limited in situ data set yielded the following best fit relationship using Type II linear least squares regression:

$$\log_{10}(C_a) = 1.564 * \log_{10}(a_{ph}(443)) + 2.283 \quad (6)$$

($r^2=0.92$; RMSE$=0.171$). Application of Eq. (6) to the GIOP-derived $a_{ph}(443)$ from MODISA yielded C_a match-ups with improved r^2 ($=0.71$ versus 0.65 in Table 2) and regression slopes (0.89 versus 0.44). However, the positive bias in MODISA-derived C_a remained (ratio of 3.77 compared to 3.62) because of the positive bias realized in the MODISA-derived $a_{ph}(443)$ (Fig. 4). We expect that additional regional tuning (e.g., Ben Mustapha et al., 2012) in subsequent studies would facilitate further reduction of these biases.

Two additional aspects of GIOP (representing all SAAs) merit discussion in the context of using its MODISA data records to study the western Arctic. First, as previously noted, MODISA $R_{rs}(\lambda)$ showed a Rayleigh-like spectral brightening in blue wavelengths as compared to in situ measurements, which we originally

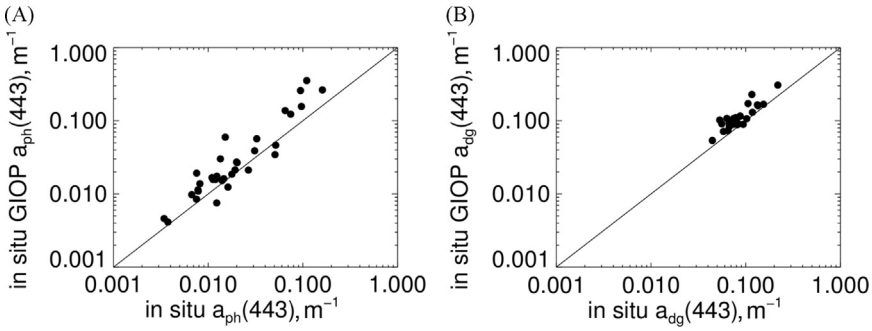

Fig. 10. GIOP-derived $a_{ph}(443)$ (A) and $a_{dg}(443)$ (B) using 11 wavelengths, rather than just MODISA wavelengths, versus in situ measured values. Type II regression statistics presented in Table 3.

anticipated would influence the GIOP retrievals. Note, the elevated $R_{rs}(\lambda)$ did not unduly affect the MBR (and thus OC3M and Stramski POC) because the bands for its calculation (i.e., $R_{rs}(488)$ and $R_{rs}(547)$) were the least affected by the overestimation (Table 2). In practice, the brightened $R_{rs}(\lambda)$ did not alter our GIOP results. The spectral dependence of the brightening mirrored the spectral absorption of CDOM (sequentially increasing with decreasing wavelength). Given that $R_{rs}(\lambda)$ and absorption are inversely proportional (Morel and Prieur, 1977), erroneously elevated blue $R_{rs}(\lambda)$ conceptually produces an underestimation of CDOM in an SAA (i.e., less absorbed blue light suggests low CDOM absorption). The model-to-in situ ratios of 1.64 for $a_{ph}(443)$ and 0.77 for $a_{dg}(443)$ support this theory. With this in mind, our demonstration that OC3M overestimated C_a in regions of high CDOM remains relevant and, if anything, understated. Naturally, the influence of ice edges (Bélanger et al., 2007) – and how adjacency effects propagate through a Rayleigh atmosphere at high latitudes – merits further investigation. Any brightening of satellite $R_{rs}(\lambda)$ bands relative to in situ measurements is uncommon – the most frequently seen biases tend towards under-estimation (Bailey and Werdell, 2006). That said, our interest was in evaluating derived biogeochemical data records. Further analysis of MODISA atmospheric correction in the western Arctic exceeds the scope of this paper.

Second, one might expect the performance of GIOP to improve with the addition of more $R_{rs}(\lambda)$ in the ultraviolet-to-visible spectral range. Future ocean color sensors, such as the NASA Pre-Aerosols, Clouds, and ocean Ecosystems (PACE) instrument, are expected to collect $R_{rs}(\lambda)$ with additional spectral resolution (National Research Council, 2011; PACE Mission Science Definition Team, 2012). Using five additional spectral bands (395, 465, 510, 560, and 625 nm) from the in situ radiometry – in addition to the MODISA bands at 412, 443, 488, 531, 547, and 667 nm – to estimate GIOP $a_{ph}(\lambda)$ and $a_{dg}(\lambda)$ improved the performance metrics for those parameters (Fig. 10, Table 3). Executing GIOP with 11 wavelengths instead of 6 improved the regression slope, RMSE, and ratio for $a_{ph}(443)$ from 1.18, 0.202, and 1.64 to 1.16, 0.184, and 1.38, respectively. Similarly, these statistics for $a_{dg}(443)$ improved from 1.05, 0.082, and 0.77 to 1.03, 0.077, and 1.33. The addition of $R_{rs}(395)$ drove the shift in bias in $a_{dg}(443)$ from negative to positive. Repeated analyses, perhaps in combination with analytical simulations using Hydrolight, for example (Mobley and Sundman, 2003), would provide additional insight into advanced spectral requirements for new satellite instruments to support ocean color Arctic research.

5. Conclusions

These results demonstrate that the pervasive positive bias in OC3M C_a estimates, and similar empirical approaches, for the Arctic Ocean reported here and previously by others, are due to the direct effect of the absorption by CDOM on remote-sensing reflectances. The resulting bio-optical signature for this region has not been well characterized in the datasets that support ocean color algorithm development for current ocean color missions. The improved performance of the semi-analytical GIOP approach in separating the in-water light absorbing components suggests that a path forward for improved ocean color applications, which satisfies climate research needs, should rely more heavily on a mechanistic understanding of the phenomena that affect light propagation in the Arctic Ocean. For example, future studies that further characterize and use phytoplankton absorption instead of just chlorophyll-*a* abundance will help improve IOP-to-C_a transfer functions in semi-analytical algorithms. Likewise, better characterization of Rayleigh-like spectral brightening of satellite data identified here suggests adjacency effects that merit further review. Furthermore, the improved performance from applying additional spectral bands to semi-analytical algorithms demonstrates the advantage of improved spectral resolution for future ocean color sensors that will be applied to Arctic and global ocean research.

Acknowledgements

The NASA Ocean Biology and Biogeochemistry (OBB) program provided support for the ICESCAPE project. Additional support was provided through an award to NASA GSFC for the Field Program Support Group. We thank the officers and crew of the USCGC Healy for their logistical and technical support that made this work possible. We thank two anonymous reviewers for their many helpful suggestions.

References

Antoine, D., Hooker, S.B., Bélanger, S., Matsuoka, A., Babin, M., 2013. Apparent optical properties of the Canadian Beaufort Sea; Part 1: observational overview and water column relationships. Biogeosciences 10 (7), 4493–4509. http://dx.doi.org/10.5194/bg-10-4493-2013.

Arrigo, K.R., Perovich, D.K., Pickart, R.S., Brown, Z.W., van Dijken, G.L., Lowry, K.E., Mills, M.M., Palmer, M.A., Balch, W.M., Bahr, F., Bates, N.R., Benitez-Nelson, C., Bowler, B., Brownlee, E., Ehn, J.K., Frey, K.E., Garley, R., Laney, S.R., Lubelczyk, L., Mathis, J., Matsuoka, A., Mitchell, B.G., Moore, G.W.K., Ortega-Retuerta, E., Pal, S., Polashenski, C.M., Reynolds, R.A., Schieber, B., Sosik, H.M., Stephens, M., Swift, J.H., 2012. Massive phytoplankton blooms under Arctic Sea ice. Science 336 (6087), 1408. http://dx.doi.org/10.1126/science.1215065.

Arrigo, K.R., van Dijken, G.L., 2011. Secular trends in Arctic Ocean net primary production. J Geophys Res 116 (C9), C09011. http://dx.doi.org/10.1029/2011jc007151.

Bailey, S.W., Franz, B.A., Werdell, P.J., 2010. Estimation of near-infrared water-leaving reflectance for satellite ocean color data processing. Opt Express 18 (7), 7521–7527. http://dx.doi.org/10.1364/OE.18.007521.

Bailey, S.W., Werdell, P.J., 2006. A multi-sensor approach for the on-orbit validation of ocean color satellite data products. Remote Sens. Environ. 102 (102), 12–23. http://dx.doi.org/10.1016/j.rse.2006.01.015.

Behrenfeld, M.J., Boss, E., Siegel, D.A., Shea, D.M., 2005. Carbon-based ocean productivity and phytoplankton physiology from space. Glob. Biogeochem. Cycles 19, GB1006. http://dx.doi.org/10.1029/2004gb002299.

Bélanger, S., Babin, M., Tremblay, J.É., 2013. Increasing cloudiness in Arctic damps the increase in phytoplankton primary production due to sea ice receding. Biogeosciences 10 (6), 4087–4101. http://dx.doi.org/10.5194/bg-10-4087-2013.
Bélanger, S., Ehn, J.K., Babin, M., 2007. Impact of sea ice on the retrieval of water-leaving reflectance, chlorophyll a concentration and inherent optical properties from satellite ocean color data. Remote Sens. Environ. 111 (1), 51–68. http://dx.doi.org/10.1016/j.rse.2007.03.013.
Ben Mustapha, S., Bélanger, S., Larouche, P., 2012. Evaluation of ocean color algorithms in the southeastern Beaufort Sea, Canadian Arctic: new parameterization using SeaWiFS, MODIS, and MERIS spectral bands. Can. J. Remote Sens. 38 (05), 535–556. http://dx.doi.org/10.5589/m12-045.
Brando, V.E., Dekker, A.G., Park, Y.J., Schroeder, T., 2012. Adaptive semianalytical inversion of ocean color radiometry in optically complex waters. Appl. Opt. 51 (15), 2808–2833. http://dx.doi.org/10.1364/AO.51.002808.
Brewin, R.J.W., Sathyendranath, S., Müller, D., Brockmann, C., Deschamps, P.-Y., Devred, E., Doerffer, R., Fomferra, N., Franz, B., Grant, M., Groom, S., Horseman, A., Hu, C., Krasemann, H., Lee, Z., Maritorena, S., Mélin, F., Peters, M., Platt, T., Regner, P., Smyth, T., Steinmetz, F., Swinton, J., Werdell, J., White Iii, G.N., 2013. The ocean colour climate change initiative: III. A round-robin comparison on in-water bio-optical algorithms. Remote Sens. Environ. , http://dx.doi.org/10.1016/j.rse.2013.09.016.
Bricaud, A., Morel, A., Babin, M., Allali, K., Claustre, H., 1998. Variations of light absorption by suspended particles with chlorophyll a concentration in oceanic (case 1) waters: analysis and implications for bio-optical models. J. Geophys. Res.: Oceans 103 (C13), 31033–31044. http://dx.doi.org/10.1029/98JC02712.
Brunelle, C.B., Larouche, P., Gosselin, M., 2012. Variability of phytoplankton light absorption in Canadian Arctic seas. J. Geophys. Res. 117, C00G17. http://dx.doi.org/10.1029/2011jc007345.
Ciotti, Á.M., Lewis, M.R., Cullen, J.J., 2002. Assessment of the relationships between dominant cell size in natural phytoplankton communities and the spectral shape of the absorption coefficient. Limnol. Oceanogr. 47 (2), 404–417. http://dx.doi.org/10.4319/lo.2002.47.2.0404.
Comiso, J.C., 2011. Large decadal decline of the arctic multiyear ice cover. J. Clim. 25 (4), 1176–1193. http://dx.doi.org/10.1175/JCLI-D-11-00113.1.
Comiso, J.C., Parkinson, C.L., Gersten, R., Stock, L., 2008. Accelerated decline in the Arctic sea ice cover. Geophys. Res. Lett. 35 (1), L01703. http://dx.doi.org/10.1029/2007gl031972.
Cota, G.F., Harrison, W.G., Platt, T., Sathyendranath, S., Stuart, V., 2003. Bio-optical properties of the Labrador Sea. J. Geophys. Res.: Oceans 108 (C7), 3228. http://dx.doi.org/10.1029/2000jc000597.
Cota, G.F., Wang, J., Comiso, J.C., 2004. Transformation of global satellite chlorophyll retrievals with a regionally tuned algorithm. Remote Sens. Environ. 90 (3), 373–377.
Dierssen, H.M., Smith, R.C., 2000. Bio-optical properties and remote sensing ocean color algorithms for Antarctic Peninsula waters. J. Geophys. Res.: Oceans 105 (C11), 26301–26312. http://dx.doi.org/10.1029/1999jc000296.
Franz, B.A., Kwiatowska, E.J., Meister, G., McClain, C.R., 2008. Moderate Resolution imaging spectroradiometer on terra: limitations for ocean color applications. APPRES 2 (1), 023525–023525-17. http://dx.doi.org/10.1117/1.2957964.
Franz, B.A., Werdell, P.J., Meister, G., Bailey, S.W., EpleeJr, R.E., Feldman, G.C., Kwiatkowskaa, E., McClain, C.R., Patt, F.S., Thomas, D., 2005. The Continuity of Ocean Color Measurements from SeaWiFS to MODIS vol. 5882, pp. 58820W–58820W-13.
Gordon, H.R., McCluney, W.R., 1975. Estimation of the depth of sunlight penetration in the sea for remote sensing. Appl. Opt. 14 (2), 413–416. http://dx.doi.org/10.1364/AO.14.000413.
Gordon, H.R., Morel, A., 1983. Remote Assessment of Ocean Color for Interpretation of Satellite Visible Imagery. Springer-Verlag, Berlin.
Granskog, M.A., Stedmon, C.A., Dodd, P.A., Amon, R.M.W., Pavlov, A.K., de Steur, L., Hansen, E., 2012. Characteristics of colored dissolved organic matter (CDOM) in the Arctic outflow in the Fram Strait: assessing the changes and fate of terrigenous CDOM in the Arctic Ocean. J. Geophys. Res. 117 (C12), C12021. http://dx.doi.org/10.1029/2012jc008075.
Guéguen, C., Guo, L., Tanaka, N., 2005. Distributions and characteristics of colored dissolved organic matter in the Western Arctic Ocean. Cont. Shelf Res. 25 (10), 1195–1207. http://dx.doi.org/10.1016/j.csr.2005.01.005.
Henson, S.A., Sarmiento, J.L., Dunne, J.P., Bopp, L., Lima, I., Doney, S.C., John, J., Beaulieu, C., 2010. Detection of anthropogenic climate change in satellite records of ocean chlorophyll and productivity. Biogeosciences 7 (2), 621–640. http://dx.doi.org/10.5194/bg-7-621-2010.
Holland, M.M., Bitz, C.M., Tremblay, B., 2006. Future abrupt reductions in the summer Arctic sea ice. Geophys. Res. Lett. 33 (23), L23503. http://dx.doi.org/10.1029/2006gl028024.
Hooker, S.B., 2010. The telescoping mount for advanced solar technologies (T-MAST). In: Morrow, J.H., Hooker, S.B., Bernhard, G., Lind, R.N., Brown, J.W. (Eds.), Advances in Measuring the Apparent Optical Properties (AOPs) of Optically Complex Waters. NASA, Greenbelt, MD, pp. 66–71.
Hooker, S.B., Heukelem, L.V., Thomas, C.S., Claustre, H., Ras, J., Schluter, L., Perl, J., Trees, C., Stuart, V., Head, E., Barlow, R., Sessions, H., Clementson, L., Fishwick, J., Llewellyn, C., Aiken, J., 2005. The Second SeaWiFS HPLC Analysis Round-Robin Experiment (SeaHARRE-2), NASA; Greenbelt, MD, 1-75.
Hooker, S.B., Lind, R.N., Morrow, J.H., Brown, J.W., 2010. The submersible bio-spherical optical profiling system (SuBOPS). In: Morrow, J.H., Hooker, S.B., Bernhard, G., Lind, R.N., Brown, J.W. (Eds.), Advances in Measuring the Apparent Optical Properties (AOPs) of Optically Complex Waters. NASA, Greenbelt, MD, pp. 17–26.
IOCCG, 2006. Remote Sensing of Inherent Optical Properties: Fundamentals, Tests of Algorithms, and Applications. In: Lee, Z.P. (Ed.), Reports of the International Ocean-Colour Coordinating Group. IOCCG, Dartmouth, Canada.
Kahru, M., Brotas, V., Manzano-Sarabia, M., Mitchell, B.G., 2011. Are phytoplankton blooms occurring earlier in the Arctic? Global Change Biol. 17 (4), 1733–1739. http://dx.doi.org/10.1111/j.1365-2486.2010.02312.x.
Kishino, M., Takahashi, M., Okami, N., Ichimura, S., 1985. Estimation of the spectral absorption coefficients of phytoplankton in the sea. Bull. Mar. Sci. 37 (2), 634–642.
Knap, A.H., Michaels, A., Close, A.R., Ducklow, H., Dickson, A.G., 1996. Protocols for the Joint Global Ocean Flux Study (JGOFS) Core Measurements JGOFS Report. UNESCO p. 170.
Kwok, R., Cunningham, G.F., Wensnahan, M., Rigor, I., Zwally, H.J., Yi, D., 2009. Thinning and volume loss of the Arctic Ocean sea ice cover: 2003–2008. J. Geophys. Res.: Oceans 114 (C7), C07005. http://dx.doi.org/10.1029/2009JC005312.
Lee, Z., Carder, K.L., Arnone, R.A., 2002. Deriving inherent optical properties from water color: a multiband quasi-analytical algorithm for optically deep waters. Appl. Opt. 41 (27), 5755–5772. http://dx.doi.org/10.1364/AO.41.005755.
Loisel, H., Lubac, B., Dessailly, D., Duforet-Gaurier, L., Vantrepotte, V., 2010. Effect of inherent optical properties variability on the chlorophyll retrieval from ocean color remote sensing: an in situ approach. Opt. Express 18 (20), 20949–20959. http://dx.doi.org/10.1364/OE.18.020949.
Maritorena, S., Siegel, D.A., Peterson, A.R., 2002. Optimization of a semianalytical ocean color model for global-scale applications. Appl. Opt. 41 (15), 2705–2714.
Matsuoka, A., Babin, M., Doxaran, D., Hooker, S.B., Mitchell, B.G., Bélanger, S., Bricaud, A., 2013a. A synthesis of light absorption properties of the Pan-Arctic Ocean: application to semi-analytical estimates of dissolved organic carbon concentrations from space. Biogeosci. Discuss. 10 (11), 17071–17115. http://dx.doi.org/10.5194/bgd-10-17071-2013.
Matsuoka, A., Hill, V., Huot, Y., Babin, M., Bricaud, A., 2011. Seasonal variability in the light absorption properties of western Arctic waters: parameterization of the individual components of absorption for ocean color applications. J. Geophys. Res. 116 (C2), C02007. http://dx.doi.org/10.1029/2009jc005594.
Matsuoka, A., Hooker, S.B., Bricaud, A., Gentili, B., Babin, M., 2013b. Estimating absorption coefficients of colored dissolved organic matter (CDOM) using a semi-analytical algorithm for southern Beaufort Sea waters: application to deriving concentrations of dissolved organic carbon from space. Biogeosciences 10 (2), 917–927. http://dx.doi.org/10.5194/bg-10-917-2013.
Matsuoka, A., Huot, Y., Shimada, K., Saitoh, S.I., Babin, M., 2007. Bio-optical characteristics of the western Arctic Ocean: implications for ocean color algorithms. Can. J. Remote Sens. 33 (6), 503–518.
McClain, C.R., 2009. A decade of satellite ocean color observations. Ann. Rev. Mar. Sci. 1 (1), 19–42. http://dx.doi.org/10.1146/annurev.marine.010908.163650.
Miller, R.L., Belz, M., Castillo, C.D., Trzaska, R., 2002. Determining CDOM absorption spectra in diverse coastal environments using a multiple pathlength, liquid core waveguide system. Cont. Shelf Res. 22 (9), 1301–1310. http://dx.doi.org/10.1016/S0278-4343(02)00009-2.
Mitchell, B.G., 1992. Predictive bio-optical relationships for polar oceans and marginal ice zones. J. Mar. Syst. 3 (1–2), 91–105.
Mitchell, B.G., Holm-Hansen, O., 1991. Bio-optical properties of Antarctic Peninsula waters: differentiation from temperate ocean models. Deep-Sea Res. Part A Oceanogr. Res. Pap. 38 (8,Äì9), 1009–1028.
Mitchell, B.G., Kahru, M., Wieland, J., Stramska, M., 2003. Determination of spectral absorption coefficients of particles, dissolved material and phytoplankton for discrete water sample. In: Mueller, J.L., Fargion, G.S., McClain, C.R. (Eds.), Inherent Optical Properties: Instruments, Characterizations, Field Measurements and Data Analysis Protocols. NASA, Greenbeldt, MD, pp. 39–64.
Mobley, C.D., Sundman, L.K., 2003. Effects of optically shallow bottoms on upwelling radiances: Inhomogeneous and sloping bottoms. Limnol. Oceanogr. 48 (1, Part 2), 329–336. http://dx.doi.org/10.4319/lo.2003.48.1_part_2.0329.
Moore, T.S., Campbell, J.W., Dowell, M.D., 2009. A class-based approach to characterizing and mapping the uncertainty of the MODIS ocean chlorophyll product. Remote Sens. Environ. 113 (11), 2424–2430. http://dx.doi.org/10.1016/j.rse.2009.07.016.
Morel, A., Prieur, L., 1977. Analysis of variations in ocean color. Limnol. Oceanogr. 22, 709–722.
Morrow, J.H., Booth, C.R., Lind, R.N., Hooker, S.B., 2010. The compact-optical profiling system (C-OPS). In: Morrow, J.H., Hooker, S.B., Bernhard, G., Lind, R.N., Brown, J.W. (Eds.), Advances in Measuring the Apparent Optical Properties (AOPs) of Optically Complex Waters. NASA, Greenbelt, MD, pp. 42–50.
Mueller, J.L., Austin, R.W. (Eds.), 1995. Ocean Optics Protocols for SeaWiFS Validation, Revision 1. NASA Goddard Space Flight Center, Greenbelt, MD.
National Research Council, 2011. Assessing Requirements for Sustained Ocean Color Research and Operations. National Academy of Sciences p. 126.
O'Reilly, J.E., Maritorena, S., Mitchell, B.G., Siegel, D.A., Carder, K.L., Garver, S.A., Kahru, M., McClain, C., 1998. Ocean color chlorophyll algorithms for SeaWiFS. J. Geophys. Res.: Oceans 103 (C11), 24937–24953. http://dx.doi.org/10.1029/98JC02160.
Pabi, S., van Dijken, G.L., Arrigo, K.R., 2008. Primary production in the Arctic Ocean, 1998–2006. J. Geophys. Res.: Oceans 113 (C8), C08005. http://dx.doi.org/10.1029/2007jc004578.
PACE Mission Science Definition Team, 2012. In: Del Castillo, C. (Ed.), Pre-Aerosol, Clouds, and Ocean Ecosystem (PACE) Mission Science Definition Team Report.
Pegau, W.S., 2002. Inherent optical properties of the central Arctic surface waters. J. Geophys. Res. 107 (C10), 8035. http://dx.doi.org/10.1029/2000jc000382.

Perovich, D.K., 1996. The Optical Properties of Sea Ice. U.S. Army Cold Regions Research and Engineering Laboratory.
Petrenko, D., Pozdnyakov, D., Johannessen, J., Counillon, F., Sychov, V., 2013. Satellite-derived multi-year trend in primary production in the Arctic Ocean. Int. J. Remote Sens. 34 (11), 3903–3937. http://dx.doi.org/10.1080/01431161.2012.762698.
Rachold, V., Eicken, H., Gordeev, V.V., Grigoriev, M.N., Hubberten, H.W., Lisitzin, A.P., Shevchenko, V.P., Schirrmeister, L., 2004. Modern terrigenous organic carbon input to the Arctic Ocean. In: Stein, R., MacDonald, R. (Eds.), The Organic Carbon Cycle in the Arctic Ocean. Springer, Berlin, Heidelberg, pp. 33–55.
Roesler, C.S., 1998. Theoretical and experimental approaches to improve the accuracy of particulate absorption coefficients from the quantitative filter technique. Limnol. Oceanogr. 43, 1649–1660.
Sauer, M.J., Roesler, C.S., Werdell, P.J., Barnard, A., 2012. Under the hood of satellite empirical chlorophyll a algorithms: revealing the dependencies of maximum band ratio algorithms on inherent optical properties. Opt. Express 20 (19), 20920–20933. http://dx.doi.org/10.1364/oe.20.020920.
Siegel, D.A., Maritorena, S., Nelson, N.B., Hansell, D.A., Lorenzi-Kayser, M., 2002. Global distribution and dynamics of colored dissolved and detrital organic materials. J. Geophys. Res. 107 (C12), 3228, http://dx.doi.org/10.1029/2004JC002762.
Siegel, D.A., Maritorena, S., Nelson, N.B., Behrenfeld, M.J., 2005. Independence and interdependencies among global ocean color properties: reassessing the bio-optical assumption. J. Geophys. Res. 110, http://dx.doi.org/10.1029/2004jc002527.
Stedmon, C.A., Amon, R.M.W., Rinehart, A.J., Walker, S.A., 2011. The supply and characteristics of colored dissolved organic matter (CDOM) in the Arctic Ocean: Pan Arctic trends and differences. Mar. Chem. 124 (1–4), 108–118. http://dx.doi.org/10.1016/j.marchem.2010.12.007.
Stramska, M., Stramski, D., 2005. Variability of particulate organic carbon concentration in the north polar Atlantic based on ocean color observations with Sea-viewing Wide Field-of-view Sensor (SeaWiFS). J. Geophys. Res. 110, C10018. http://dx.doi.org/10.1029/2004jc002762.
Stramska, M., Stramski, D., Hapter, R., Kaczmarek, S., Sto, Joanna, 2003. Bio-optical relationships and ocean color algorithms for the north polar region of the Atlantic. J. Geophys. Res. 108 (C5), 3143. http://dx.doi.org/10.1029/2001jc001195.
Stramski, D., Reynolds, R.A., Babin, M., Kaczmarek, S., Lewis, M.R., Röttgers, R., Sciandra, A., Stramska, M., Twardowski, M.S., Franz, B.A., Claustre, H., 2008. Relationships between the surface concentration of particulate organic carbon and optical properties in the eastern South Pacific and eastern Atlantic Oceans. Biogeosciences 5 (1), 171–201. http://dx.doi.org/10.5194/bg-5-171-2008.
Stramski, D., Reynolds, R.A., Kahru, M., Mitchell, B.G., 1999. Estimation of particulate organic carbon in the ocean from satellite remote sensing. Science 285 (5425), 239–242. http://dx.doi.org/10.1126/science.285.5425.239.
Szeto, M., Werdell, P.J., Moore, T.S., Campbell, J.W., 2011. Are the world's oceans optically different? J. Geophys. Res. 116, http://dx.doi.org/10.1029/2011jc007230 C00H04, http://dx.doi.org/10.1029/2011jc007230.
Van Heukelem, L., Thomas, C.S., 2001. Computer-assisted high-performance liquid chromatography method development with applications to the isolation and analysis of phytoplankton pigments. J. Chromatogr. A 910 (1), 31–49. http://dx.doi.org/10.1016/S0378-4347(00)00603-4.
Wang, J., Cota, G.F., 2003. Remote-sensing reflectance in the beaufort and chukchi seas: observations and models. Appl. Opt. 42 (15), 2754–2765.
Wang, M., Overland, J.E., 2009. A sea ice free summer Arctic within 30 years? Geophys. Res. Lett. 36 (7), L07502. http://dx.doi.org/10.1029/2009gl037820.
Warren, S.G., 1982. Optical properties of snow. Rev. Geophys. 20 (1), 67–89. http://dx.doi.org/10.1029/RG020i001p00067.
Warren, S.G., Brandt, R.E., Grenfell, T.C., 2006. Visible and near-ultraviolet absorption spectrum of ice from transmission of solar radiation into snow. Appl. Opt. 45 (21), 5320–5334. http://dx.doi.org/10.1364/AO.45.005320.
Werdell, P.J., Bailey, S.W., 2005. An improved in-situ bio-optical data set for ocean color algorithm development and satellite data product validation. Remote Sens. Environ. 98 (1), 122–140.
Werdell, P.J., Franz, B.A., Bailey, S.W., Feldman, G.C., Boss, E., Brando, V.E., Dowell, M., Hirata, T., Lavender, S.J., Lee, Z., Loisel, H., Maritorena, S., Mélin, F., Moore, T. S., Smyth, T.J., Antoine, D., Devred, E., d'Andon, O.H.F., Mangin, A., 2013a. Generalized ocean color inversion model for retrieving marine inherent optical properties. Appl. Opt. 52 (10), 2019–2037.
Werdell, P.J., Franz, B.A., Lefler, J.T., Robinson, W.D., Boss, E., 2013b. Retrieving marine inherent optical properties from satellites using temperature and salinity-dependent backscattering by seawater. Opt. Express 21 (26), 32611–32622. http://dx.doi.org/10.1364/OE.21.032611.
Werdell, P.J., Proctor, C.W., Boss, E., Leeuw, T., Ouhssain, M., 2013c. Underway sampling of marine inherent optical properties on the Tara Oceans expedition as a novel resource for ocean color satellite data product validation. Methods Oceanogr. 7, 40–51. http://dx.doi.org/10.1016/j.mio.2013.09.001.
Zaneveld, J.R., Barnard, A., Boss, E., 2005. Theoretical derivation of the depth average of remotely sensed optical parameters. Opt. Express 13 (22), 9052–9061. http://dx.doi.org/10.1364/OPEX.13.009052.
Zheng, G., Stramski, D., Reynolds, R.A., 2014. Evaluation of the Quasi-Analytical Algorithm for estimating the inherent optical properties of seawater from ocean color: Comparison of Arctic and lower-latitude waters. Remote Sensing Environ. 155 (0), 194–209. http://dx.doi.org/10.1016/j.rse.2014.08.020.